RESEARCH PAPER

A 1D Hypoplastic constitutive model for expansive soils

Carlos Eduardo Grandas Tavera[1] (ID) · Antonia Nitsch[1,2] · Jan Machaček[2,3]

Abstract

This paper presents a simple hypoplastic constitutive model that describes the essential features of the material behaviour of partially saturated clayey soils observed in oedometric compression tests. The model is formulated in terms of net stress and degree of saturation. The total strain rate is decomposed into a portion related to the changes in saturation and a portion for the evolution of net stress. However, no distinction is made between plastic and elastic strains. With this strain rate decomposition, the maximum swelling strain/stress are obtained by simulating wetting processes under constant stress/strain conditions. In addition to the void ratio, the model includes two scalar variables to track the loading history (preloading). The calibration of the model constants using common laboratory tests is discussed. Confined and unconfined swelling tests under oedometric conditions with subsequent loading and unloading phases carried out on three different materials were satisfactorily simulated by the model. Its promising results call for an extension to a 3D formulation.

Keywords Constitutive model · Expansive soils · Hypoplasticity · Partial saturation · Swelling

1 Introduction

Some rocks and soils tend to expand upon wetting due to their content of swellable clay minerals. They are commonly referred to as expansive geomaterials. Swelling can manifest itself in the form of swelling deformations or swelling stresses. While the tendency of a material to swell depends on its mineralogical composition, the swelling phenomenon (development of swelling strain or swelling stress) is largely dependent on the mechanical and hydraulic boundary conditions to which the material is subjected as well as the material properties. Reciprocally, the material properties are also affected by changes in water content. An adequate prediction of this hydro-mechanical coupled material behaviour, especially the maximum stresses or strains that can be reached during wetting, is essential for a reliable design of underground structures in contact with or embedded in expansive geomaterials.

In some practical cases, those predictions are obtained from semi-empirical extrapolations of results from laboratory tests following the Huder-Amberg-method [16] or similar according to the swelling law by Grob [13]. This law, however, focuses on the estimation of the expected deformation during unloading processes in the fully saturated state (i.e. a change in the mechanical boundary conditions) and does not consider any time effects. Further developments of this fundamental law have been implemented in several FE codes to analyze problems related to tunneling and swelling rocks and soils [3, 15]. At their basis, these models often consider a separate additional strain component for swelling in an elasto-plastic framework.

On the other hand, sophisticated constitutive models based on the Barcelona Basic Model (BBM) [1], which

✉ Carlos Eduardo Grandas Tavera
carlos.grandastavera@b-tu.de

✉ Antonia Nitsch
antonia.nitsch@rub.de

Jan Machaček
jan.machacek@tu-darmstadt.de

[1] Department of Architecture, Civil Engineering and Urban Planning, Chair of Soil Mechanics and Foundations/Geotechnical Engineering, Brandenburgische Technische Universität Cottbus-Senftenberg, Cottbus, Germany

[2] Department of Civil and Environmental Engineering, Chair of Soil Mechanics, Foundation Engineering and Environmental Geotechnics, Ruhr Universität Bochum, Bochum, Germany

[3] Department of Civil and Environmental Engineering, Institute of Geotechnics, Technische Universität Darmstadt, Darmstadt, Germany

extends the capabilities of the CamClay model [34], have been used over the last decades to simulate the mechanical response of partially saturated soils during the installation of geotechnical constructions, e.g. by Toprak et al. [39].

The BBM can simulate the most prominent features of unsaturated soils like the apparent increase of the preconsolidation pressure due to partial saturation as well as the soil expansion or soil collapse upon changes in the degree of saturation. However, some important aspects of the behaviour of expansive soils could not be captured by the BBM as the model was not originally developed for materials with swellable clay minerals. Missing features are the influence of the loading history on the swelling strains and the swelling stresses, the reduction of the elastic stiffness with increasing saturation, and the strain accumulation upon wetting-drying cycles [2, 10, 12]. To improve the response of the BBM for expansive soils during wetting-drying cycles, Gens and Alonso [2, 12] introduced the concept of microstructure into the BExM model. The macrostructural deformation due to wetting of an expansive soil is assumed to be a mechanical response to reversible strains in the microstructure which manifests itself in the evolution of the pore structure from a bi- to a mono-modal distribution [2, 12]. Another approach extending the BBM was followed by Dieudonne et al. [10] amongst others [9, 33], who introduced the concept of microstructure in the hydraulic model instead of the mechanical model. Similar efforts for bi-modal soil water retention curves (SWRC) have also been recently introduced in other elasto-plastic frameworks, e.g. by Bosch et al. [6].

Although these extended models show promising simulation results, they require new material constants and initial state variables, some of which are difficult to determine when addressing practical geotechnical problems. Furthermore, the assumption of a bimodal pore size distribution does not apply to all expansive materials, e.g. clay shales have a rather monomodal pore size distribution as has been shown for Callovo-Oxfordian clay shale by Mohajerani et al. [25] and Opalinus clay shale by Seiphoori et al. [38].

Until now, little efforts have been made to describe the behaviour of expansive geomaterials with constitutive models outside of elasto-plastic frameworks. A hypoplastic model for unsaturated soils was introduced by Mašín and Khalili [23], however it does not allow simulations of expansive geomaterials. Adopting some concepts from existing models, this paper presents a novel 1D constitutive model in the framework of hypoplasticity to describe the most essential features of the behaviour of expansive soils. The model's development takes a phenomenological approach and aims to facilitate the material calibration process. Rate dependency, creep, anhydritic swelling,

anisotropy or cementation are not considered. The model is formulated in terms of *net stress* (excess of total stress over air pressure) and effective degree of saturation. The preloading state defines a boundary for the reversible material response (analogously to a yield surface) which is assumed to evolve with the deformation and the changes in saturation. The primary consolidation and the evolution of swelling over time are out of the scope of this paper since they are related to the transport of water and, therefore, scale dependent. Hence, and contrary to other approaches [18, 21], they should be considered at the finite element level and not at the material level [27]. One novelty of the model lies in the linking of the material behavior during wetting (development of swelling strain or stress) with the preloading state instead of the widely used correlation of the maximum swelling stress/strain with the dry density, cf. [24, 37, 43, 45].

Deviating from the BBM/BExM, the proposed model uses the degree of saturation instead of the suction, which greatly simplifies many of the model's evolution equations. Although the degree of saturation also determines the current state, the constitutive model handles it as a *given* variable because its evolution is governed by the mass balance at the finite element (and not at the material point) level. This allows any hydraulic constitutive relation between suction and degree of saturation to be linked. In the model, the strain rate is divided into two parts: one is related to changes in the degree of saturation of the material while the other one is used for the evolution of net stress. This decomposition allows to predict both swelling strains and swelling stresses, depending on the mechanical and hydraulic boundary conditions. The saturation driven strain can lead to irreversible strain accumulation even for stresses that are much smaller than the preloading stress. For constant volume conditions, the strain decomposition produces an increase of stress (swelling pressure). Adopting the concept of overstress by Olszak and Perzyna [32] to quantify the proximity of the current stress to the preloading stress, the model can distinguish between loading and unloading using a single equation. On this basis, the proposed constitutive model can predict both, swelling strains and swelling stresses, loading/unloading as well as combinations thereof for different degrees of saturation with a single set of only seven material parameters.

The paper is structured as follows: First, the constitutive model is introduced in Sect. 2, with a common approach to simulate loading and unloading/reloading paths on oedometric tests. The constitutive equations are stepwise extended to include the influence of saturation on the first loading, the reduction of stiffness with wetting, and the saturation driven swelling strain rate to describe unconfined and confined swelling paths. The evolution equations for the state variables that track the loading history and the

parameters of the proposed model are introduced thereafter. An detailed discussion of the model with focus on the main mechanisms is presented in Sect. 3. The determination of the material parameters and their significance is discussed in detail in Sect. 4. To evaluate the performance of the model, laboratory tests on three different materials were simulated and their results are contrasted in Sect. 5. Finally, a conclusion is drawn in Sect. 6.

2 Constitutive model

2.1 Oedometric compression: loading and unloading

Similar to the approach by Niemunis et al. [28], the model starts with the common description of an oedometric loading and unloading/reloading process consisting of two equations:

$$
\begin{cases}
\ln\dfrac{1+e_0}{1+e} = \lambda \ln\dfrac{\sigma}{\sigma_0} & \text{or} \quad \dot\sigma = \dfrac{\sigma}{\lambda}\dot\epsilon \quad \text{for loading,} \\[2mm]
\ln\dfrac{1+e_0}{1+e} = \kappa \ln\dfrac{\sigma}{\sigma_0} & \text{or} \quad \dot\sigma = \dfrac{\sigma}{\kappa}\dot\epsilon \\[2mm]
& \qquad\qquad \text{for unloading/reloading,}
\end{cases}
\tag{1}
$$

where λ and κ are the first loading index and the swelling index, respectively. Note that although Eq. (1) is given in a 1D formulation, under oedometric conditions σ corresponds to the vertical (axial) stress and not the mean effective stress. This definition is used consistently in the following. In this paper, we adopt the logarithmic strain $\epsilon = \ln\dfrac{1+e_0}{1+e}$ and the geotechnical conventions, where compressive stress and strain are positive. The values (σ_0, e_0) represent an arbitrary point from which the deformation is to be measured. In Eq. (1) both points (σ_0, e_0) and (σ, e) must lie on the same (loading or unloading) branch. When using the rate form of Eq. (1) for loading, the first (virgin) compression line is defined as the curve in the $\ln(1+e) - \ln\sigma-$space with slope λ passing through a fixed *reference* point (σ_d, e_d). We denote this line as the B-line, see Fig. 1.

Following the concept of overstress by Olszak and Perzyna [32], we consider the response of the material to be reversible for stresses within a certain bounding stress $\sigma_B(e)$. The bounding stress is the stress corresponding to the current void ratio e on the B-line, see Fig. 1.

Loading beyond that bounding stress results in anelastic flow. The proximity of the current net stress σ to the bounding stress σ_B is expressed by the so called overconsolidation ratio $OCR = \sigma_B/\sigma$. States (σ, e) on the left hand side of the B-line ($OCR > 1$) in Fig. 1 are called
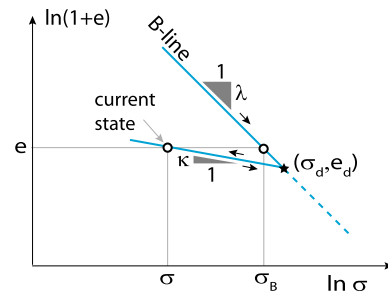

Fig. 1 Idealized loading and unloading/reloading paths, B-line with reference point (σ_d, e_d), and definition of the bounding stress σ_B corresponding to the current void ratio e

overconsolidated whereas those on the B-line ($OCR = 1$) are called *normal consolidated*. Using the OCR, Eq. (1) can be approximated by a single hypoplastic equation

$$
\dot\sigma = \frac{\sigma}{\kappa}\left(\dot\epsilon - Y OCR^{-m}|\dot\epsilon|\right) \quad \text{with}
$$
$$
Y = \frac{\lambda - \kappa}{\lambda}, \quad OCR = \sigma_B/\sigma.
\tag{2}
$$

The factor $Y OCR^{-m}$, with $m > 1$, allows to simulate both elastic unloading/reloading and anelastic loading without the need of switching between equations in Eq. (1):

- For *overconsolidated* (elastic) states $OCR > 1$, the factor $Y OCR^{-m}$ in Eq. (2) becomes negligible, and the expression $\dot\sigma = \dfrac{\sigma}{\kappa}\dot\epsilon$ from Eq. (1) for unloading/reloading is recovered.

- For *normal consolidated* states $OCR \approx 1$ and $\dot\epsilon > 1$, Eq. (2) simplifies to $\dot\sigma = \dfrac{\sigma}{\kappa}\left(1 - \dfrac{\lambda - \kappa}{\lambda}\right)\dot\epsilon$, which is identical to the expression $\dot\sigma = \dfrac{\sigma}{\lambda}\dot\epsilon$ for loading in Eq. (1).

The material constant m in Eq. (2) enforces the change from elastic to anelastic material behavior: the higher m, the sharper the transition from elastic to anelastic behavior. From the authors' experience, $m = 6$ is an applicable choice for most materials. Notice that states with $OCR < 1$ (beyond the bounding stress σ_B) are also allowed by Eq. (2).

2.2 Oedometric compression: influence of saturation

Several experimental campaigns [22, 26, 30] show that after oedometric compression up to high stresses (exceeding the preconsolidation stress) under constant suction, samples with different degrees of saturation approach a *unique* compression line: the so called Normal Compression Curve (NCC), see Fig. 2. Even nearly dry samples seem to approach the NCC at very high stresses. Therefore,
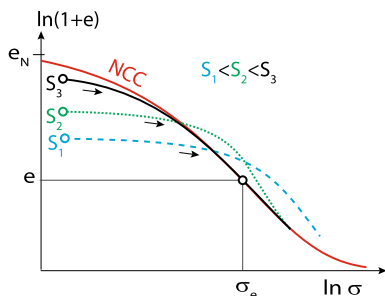
Fig. 2 Idealized oedometric compression paths at constant suction for different initial degrees of saturation $S_1 < S_2 < S_3$. After compression up to stresses exceeding the preconsolidation stress, all samples approach the Normal Compression Curve NCC
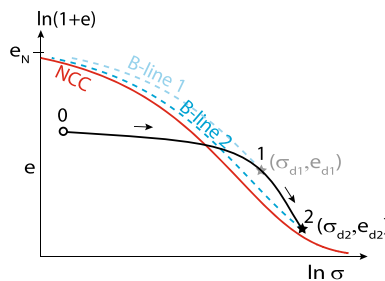

Fig. 3 Compression of a sample with low degree of saturation: shift of the B-line from state 1 to 2 during compression at high stresses to approximate NCC

the NCC can be thought as an attractor: a line reached upon compression regardless of the initial state and the degree of saturation. The concept of a NCC is incorporated into the proposed constitutive model through a unique function $\sigma_e(e)$ that returns the stress σ_e on the NCC for a given void ratio e.

This unique function $\sigma_e(e)$ can be described by the Butterfield's [7] Eq. $\ln\dfrac{1+e_0}{1+e} = \Lambda \ln\dfrac{\sigma_e}{\sigma_0}$ as commonly done for compression lines of clayey materials. Therein, three material constants are required: σ_0, e_0 and the slope Λ. To prevent negative or excessively large void ratios at high and low stresses, respectively, a 1D formulation of Bauer's [5] equation is used in the present work to describe the NCC:

$$\sigma_e(e) = h_s[-\ln(e/e_N)]^{1/n}. \tag{3}$$

Compared with the Butterfield's equation, the main advantage of Eq. (3) is that it remains valid over a wider stress range $0 \le \sigma_e < \infty$, see Fig. 10. In addition, the flexibility of the Bauer's formula (Eq. (3)) permits a better approximation the experiments requiring the same number of material constants than the Butterfield's one: the stress at the inflection point h_s (in kPa), the void ratio at zero stress e_N, and the exponent n.

Notice that the higher the degree of saturation, the sooner the NCC is reached upon compression, see Fig. 2. For fully saturated samples $S = 1$, the first compression line from Eq. (2) and the NCC should become almost identical. Experiments indicate that samples with lower degrees of saturation reach the NCC line at higher pressures [22, 26, 30]. To incorporate this behaviour into the constitutive model, the compression of a sample with a low degree of saturation is considered, see Fig. 3. It is assumed that at the beginning of the compression (from point 0 to 1), the sample behaves elastically (reloading along a κ–slope) until the B-line is reached. Along the B-line, the sample follows the first loading path with a slope $\lambda(e)$. However, in order to reach the NCC upon further

compression, the B-line must be *shifted* towards the NCC. To achieve this, the reference point (σ_d, e_d), which fixes the position of the B-line, must move towards the NCC during compression (from point 1 to 2). Hence, the reference point (σ_d, e_d) becomes a state variable that evolves with the loading history. The evolution of σ_d and e_d will be discussed in Sect. 2.6.

It is further assumed that the path followed during first compression along the B-line is affine to the NCC. This means that for a given void ratio e, the slope $\lambda = -\dfrac{\sigma}{1+e}\dfrac{\mathrm{d}e}{\mathrm{d}\sigma}$ for the first compression (i.e. the B-line) is identical to the slope $\lambda(e)_{NCC}$ of the NCC. By computing the derivative $\dfrac{\mathrm{d}e}{\mathrm{d}\sigma_e}$ from Eq. (3), we obtain the slope λ as

$$\lambda = \lambda(e) = \lambda_{NCC}(e) = n(\sigma_e/h_s)^n\frac{e}{1+e} \quad \text{with} \quad \lambda > \kappa. \tag{4}$$

Notice that, in contrast to the BBM [1] or other elastoplastic formulations, e.g. by Bosch et al. [6], the slope $\lambda(e)$ does not depend on the suction (or on the degree of saturation). The apparent dependency of λ on the suction is accounted for as the slope resulting from the transition from κ to λ with a shifting B-line in this model.

2.3 Unloading/reloading for partial saturation

Experiments further show a pronounced reduction of the elastic stiffness with increasing degree of saturation [26, 29, 30]. To take this into account, the dependency of $\kappa(S)$ on the degree of saturation S is included in the model by assuming a simple linear interpolation between dry and saturated conditions:

$$\kappa(S) = \kappa_d + S(\kappa_w - \kappa_d). \tag{5}$$

Therein, κ_d denotes the swelling index at dry and κ_w at fully saturated conditions, respectively. Figure 4 shows the loading and unloading behavior for two samples with different degrees of saturation $S_1 < S_2$,
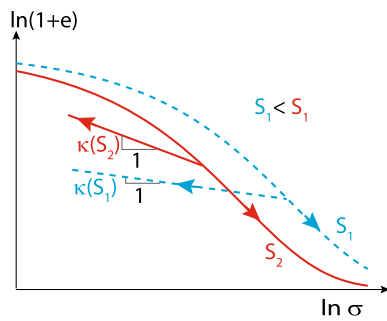
Fig. 4 Swelling indexes $\kappa(S_1)$ and $\kappa(S_2)$ for samples with degrees of saturation S_1 and S_2, respectively. The lower the degree of saturation, the higher the elastic stiffness. For $S_1 < S_2$, $\kappa(S_1) < \kappa(S_2)$ holds

Equation (5) bears the problem that κ_d is a theoretical value (unloading stiffness at degree of saturation $S = 0$) which is difficult to measure in the laboratory. Considering that a nearly *dry* sample under atmospheric conditions has a residual water content, Eq. (5) can be reformulated in analogy to the concept of the effective degree of saturation as follows:

$$\kappa(S^e) = \kappa_{\text{ref}} + S^e(\kappa_w - \kappa_{\text{ref}}) \tag{6}$$

Therein, κ_{ref} denotes the unloading stiffness measured in the laboratory in a reference degree of saturation S_{ref}. $S^e = (S - S^r)/(1 - S^r)$ is the effective degree of saturation and S^r the residual degree of saturation. For the determination of $\kappa_{\text{ref}} = \kappa(S_{\text{ref}})$, it is strongly recommended to select the driest possible state of the material $S_{\text{ref}} = S^r$, or, in other words, a state as close as possible to $S^e = 0$. The illustration of the saturation dependent unloading stiffness $\kappa(S)$ in Fig. 4 also applies to the interpolation with the effective degree of saturation $\kappa(S^e)$.

Notice that the saturation dependent swelling index of Eq. (6) differs from the constant elastic stiffness of the original formulations of BBM/BExM [1, 12]. However, more recent formulations also consider the swelling index as a function of suction (hence of degree of saturation) [8, 36, 42].

2.4 Unconfined swelling

The extensions introduced in the following account for deformations caused by changes in the degree of saturation at constant net stresses. The relation between void ratio e and water content w in partial saturated samples during drying-wetting tests has been widely studied [11, 14, 40]. After a few drying-wetting cycles at constant net stress, the samples followed a nearly identical path in the $e - w-$space, see Fig. 5. Starting at very low water contents $w \leq w_s$ (where w_s is the shrinkage limit) the samples swelled upon wetting ($\dot{S} > 0$) until a given void ratio e_w was reached at full saturation ($S = 1$). After a subsequent

drying process, the void ratio reduced up to e_s (the void ratio at the shrinkage limit). Thus, the void ratios e_w and e_s can be seen as limit values for the void ratio during wetting and drying processes, respectively. Experiments performed at different stress levels show that the limits e_w and e_s are both functions of the net stress and the loading history as presented in Fig. 6 and Sect. 2.6.

To include these observation into the constitutive model, the total strain rate $\dot{\epsilon}$ is decomposed into a portion $\dot{\epsilon}^w$ and a portion $\dot{\epsilon}^h$: $\dot{\epsilon} = \dot{\epsilon}^h + \dot{\epsilon}^w$. The strain rate portion $\dot{\epsilon}^w$ is related the changes in the degree of saturation (*the saturation driven strain rate*). The remaining strain rate portion $\dot{\epsilon}^h$ is used to describe the evolution of the net stress, so that Eq. (2) is rewritten as:

$$\dot{\sigma} = \frac{\sigma}{\kappa}\left(\dot{\epsilon}^h - Y\text{OCR}^{-m}|\dot{\epsilon}^h|\right) \quad \text{with} \quad \dot{\epsilon}^h = \dot{\epsilon} - \dot{\epsilon}^w. \tag{7}$$

Notice that for unconfined swelling $\dot{\epsilon}^w \neq 0$, the portion $\dot{\epsilon}^h$ must be zero to satisfy the condition of constant net stress $\dot{\sigma} = 0$ in Eq. (7). Thus, the relationship between the deformation changes $\dot{\epsilon} = \dot{\epsilon}^h + \dot{\epsilon}^w$ and the change in the degree of saturation $\dot{S}$ is obtained from the above mentioned observations. As for Eq. (6), the effective degree of saturation S^e is used rather than the (total) degree of saturation S. This choice reflects the difficulty attached to the evaluation of swelling processes on nearly dry samples under atmospheric conditions. By choosing S^e, only swelling/shrinking processes that ranges from this (reference) state to full saturation are considered in the model. During wetting $\dot{S}^e > 0$, the volume of the sample increases $\dot{\epsilon}^w < 0$ until the void ratio reaches the limiting value $e \to e_w$ at full saturation, i.e. $\dot{\epsilon}^w \sim (e - e_w)\dot{S}^e$. During drying $\dot{S}^e < 0$, the volume of the sample reduces $\dot{\epsilon}^w > 0$ until the limiting void ratio $e \to e_s$ is reached at *nearly* dry conditions, i.e. $\dot{\epsilon}^w \sim (e_s - e)\dot{S}^e$. These two processes can be described by a single evolution equation:

$$\begin{aligned} \dot{\epsilon}^w = -b\frac{e}{(1+e)}\Big[(e_w - e)(S^e)^2\langle\dot{S}^e\rangle \\ + (e_s - e)(1 - S^e)^2\langle-\dot{S}^e\rangle\Big] \end{aligned} \tag{8}$$

where b is a material constant that controls the shape of the $e - w-$path[1]. The Macaulay brackets are defined as $\langle\sqcup\rangle = (\sqcup + |\sqcup|)/2$. The factors $(S^e)^2$ and $(1 - S^e)^2$ decelerate the evolution of $\dot{\epsilon}^w$ upon changes in the effective degree of saturation at nearly dry and fully saturated states, respectively, as observed in Fig. 5.

Notice that the maximum strain reached at the end of a wetting process depends on the net stress. To illustrate this

---

[1] Instead of b, one may use two factors b_1 and b_2 for the first and the second terms in Eq. (8), respectively, to describe drying and wetting paths independently.
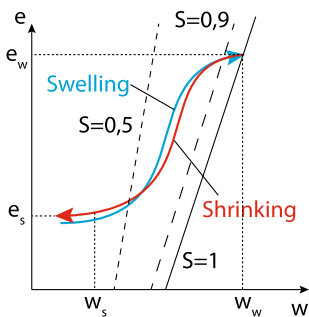
Fig. 5 Idealized evolution of the void ratio upon drying and wetting at constant net stress after Estabragh et al. [11]
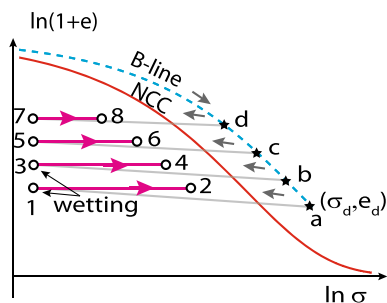
Fig. 7 Idealization of confined swelling tests of samples prepared at different preconsolidation pressures
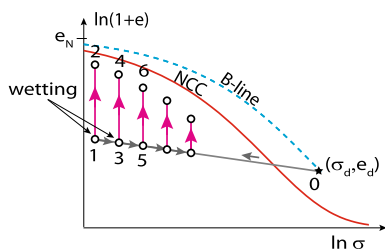
Fig. 6 Idealization of different unconfined swelling tests for samples wetted under different loads

observation, consider the set of idealized swelling experiments in Fig. 6. A sample is statically compacted under σ_d and reaches the void ratio e_d (point 0). After unloading (from 0 to 1), the saturation is increased and the sample swells under constant net stress (from 1 to 2). At point 2, the void ratio reaches its limit value e_w and the *saturation driven strain rate* vanishes according to Eq. (8). If the wetting process were initiated at a higher stress (e.g. path 0-1-3), the void ratio would increase under constant net stress and would reach the point 4 at $e = e_w$. The final swelling strain along the path 0-1-3-4 (at a higher stress) is smaller than the one along the path 0-1-2 (at a lower stress). Even smaller swelling strains would be obtained at higher stresses, e.g. path 0-1-5-6.

Since at the end of all these paths the limiting void ratio e_w is reached, a relation $e_w(\sigma)$ for samples prepared at the same preloading (σ_d, e_d) can be constructed as the curve connecting the end points 2, 4, 6, $\cdots$. This curve, which is a reinterpretation of the commonly reported relation of $\epsilon_{max} \sim \rho_d$ [43, 45], can then be used to predict the *maximum swelling strain* ϵ_{max} under constant stress σ for a sample prepared at given preloading σ_d. Note that this hypothetical connection line shows an affinity to the NCC.

2.5 Confined swelling

In the proposed model, the maximum swelling pressure σ_{max} is obtained as a confined swelling process: during wetting, the saturation driven strain increases $\dot{\epsilon}^w \neq 0$ until

the asymptotic value $e = e_w$ is reached, while the total strain is constrained by the constant volume condition $\dot{\epsilon} = \dot{\epsilon}^w + \dot{\epsilon}^h = 0$. The remaining strain portion $\dot{\epsilon}^h = -\dot{\epsilon}^w$ induces the changes of the net stress according to Eq. (7).

Due to its practical importance, predictions of the maximum swelling pressure σ_{max} have been widely studied over the last decades. Those studies usually include experiments on dry samples subjected to full saturation under constant volume conditions.

The maximum swelling pressure σ_{max} thus determined is often linked to the dry density ρ_d using exponential relationships $\sigma_{max} \sim \exp(\rho_d)$, whereby ρ_d is evaluated the beginning of the wetting process [24, 37, 43, 45]. However, a more evident relation can be found between σ_{max} and the preloading stress σ_d, i.e. the maximum stress at which the dry sample was subject before wetting.

To illustrate this relationship, consider a set of idealized constrained swelling tests shown in Fig. 7. Similar to the procedure described in Fig. 6, a nearly dry sample is statically compacted under a vertical net stress σ_d reaching the void ratio e_d (point a). After unloading (from a to 1), the saturation increases while the volume is kept unchanged. Since the tendency of the sample to swell is restricted (constant volume conditions), the measured stress increases (from point 1 to 2). The final value of the stress (at point 2) is the maximum swelling pressure σ_{max} that corresponds to the preloading σ_d (or the density given by e_d). If a second nearly dry sample is preloaded up to a lower stress (point b), then unloaded (from b to 3), and finally subjected to a wetting process (from 3 to 4), the maximum swelling pressure (at point 4) would be smaller than the one reached along the path a-1-2. Therefore, the maximum swelling pressure is directly related to the preloading stress. Analogously to the previous Section 2.4, a curve connecting the end points of the swelling process 2, 4, 6, 8 can be constructed. This curve is also affine to NCC. This relationship can be found in several experimental campaigns. For example, Fig. 8 presents the preloading stress σ_d and its corresponding maximum swelling stress σ_{max} for different materials [4, 17, 43].
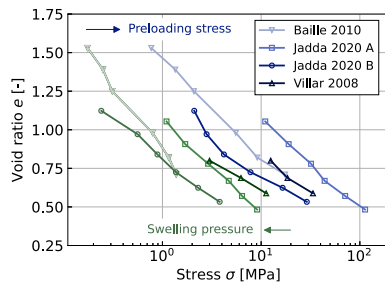
Fig. 8 Maximum swelling σ_{max} and preloading pressures σ_d for different materials [4, 17, 43]

It can be seen that for a given material, the maximum swelling stress $\sigma_{max}(e)$ at a given void ratio e is always smaller than the corresponding preloading stress $\sigma_d(e)$. In addition, by connecting all preloading stresses σ_d of a single material, we obtain a line that is nearly parallel to the line connecting the corresponding maximum stresses σ_{max}. Since the preloading is carried out by increasing the vertical stress (oedometric loading), the former line can be interpreted as the B-line (see Fig. 7). On the other hand, the second line connects the states at the end of wetting processes (where the void ratio reaches the limiting value $e = e_w$ at $S = 1$). The final values for each confined swelling test can be related to as a respective third line, which is introduced as the w-line. Note, that in contrast to NCC, the w-line is not unique. It differs slightly for each test, since the magnitude of the saturation driven strain ϵ_w, which causes the development of swelling pressure, depends on the initial void ratio. However, the slope of each individual w-line is very similar and is affine to the connecting line, which in turn is affine to the B-line.

This simplification suggests that the w-line can be used not only to predict the maximum swelling pressure σ_{max}, but also the maximum swelling strain ϵ_{max}, where the same affinity of the line connecting the final states e_w and the B-line was observed, see Sect. 2.4).

Swelling under confined and unconfined conditions is idealized in the proposed model by using three characteristic lines, see Fig. 9. A nearly dry sample is compressed (from point 0 to 1) under the stress σ_d, then unloaded (from 1 to 3), and finally subjected to a wetting process. The w-line ($e = e_w$) can be reached either upon free (from 3 to 4a, left) or constrained (from 3 to 4b, right) swelling.

2.6 Characteristic curves

In the previous sections, three characteristic curves in the $e - \ln\sigma-$space have been introduced:

- the B-line: the first (or) virgin compression line $\sigma_B(e, sv)$,
- the NCC: an attractor $\sigma_e(e)$ reached after long compression regardless of the initial state of the sample, and
- the w-line: a state reached by the sample at the end of a full saturation process $\sigma_w(e, sv)$.

Note that the B-line and the w-line are state sv dependent, i.e. they evolve with the change of deformation (change in void ratio) and saturation. These lines constitute the core of the proposed material model, see Fig. 10. For the complete description of the model, however, the relative position of those lines in $e - \ln\sigma-$space is required. Since the NCC (Eq. (3)) is an attractor, its position is given by the material constants e_N, h_s and n and remains constant during any loading process. In contrast to the NCC, the B-line and the w-line evolve with the loading history. Based on the experiments already referred to in Sect. 2.4 and 5, we assume a) that the B-line lies always on the right hand side of the w-line and b) that the NCC is located between the B-line and the w-line as shown in Fig. 10. That means, that for any given void ratio e

$$\sigma_w(e) \leq \sigma_e(e) \leq \sigma_B(e) \tag{9}$$

holds. The bounding stress $\sigma_B(e)$ is the stress corresponding to the current void ratio e on the B-line. The B-line
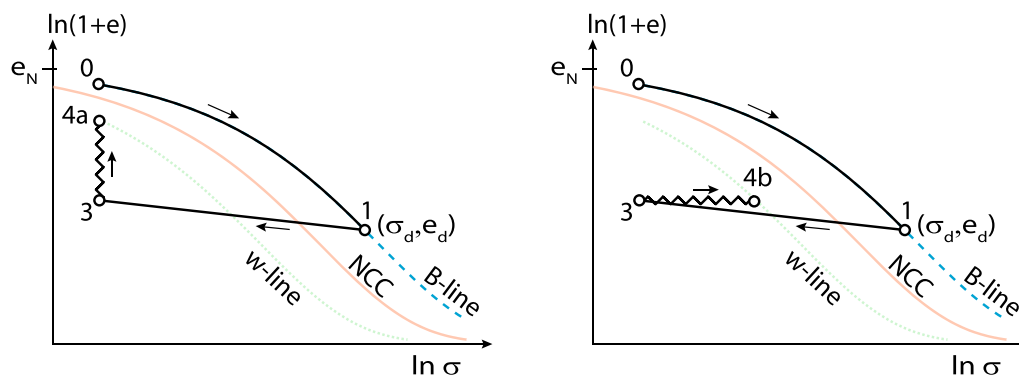
Fig. 9 Idealization of swelling processes: at the end stage of wetting, the w-line can be reached either by keeping the stress (left) or the volume (right) constant
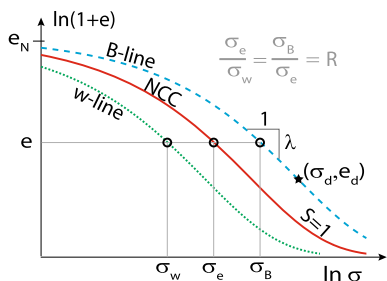
Fig. 10 Three characteristic lines of the model and their relative position described by the equivalent stress σ_e on the Normal Compression Curve NCC, the bounding stress σ_B on the B-line and stress reached for full saturation process σ_w for any void ratio e

tracks the material's loading history and is affine to the NCC (Eq. (3)).

Thus, the B-line

$$\sigma_B(e) = R \cdot \sigma_e(e) = R \cdot h_s[-\ln(e/e_N)]^{1/n} \tag{10}$$

has the same constants e_N, h_s and n as the NCC, but is shifted to the right of the NCC by a factor R. The factor R is found from the condition that the B-line (Eq. (10)) passes through (σ_d, e_d):

$$R = \frac{\sigma_d}{h_s}[-\ln(e_d/e_N)]^{-1/n} = \frac{\sigma_B}{\sigma_e}. \tag{11}$$

Therefore, the preloading state (σ_d, e_d) controls the position of the B-line on which the bounding stress σ_B is computed. The evolution of the preloading (σ_d, e_d) is given in Sect. 2.6.

We assume that the w-line is also affine to the NCC, i.e. it has the same constants, but it is shifted to the left by the *same* factor R in Eq. (11)

$$\sigma_w(e) = \sigma_e(e)/R, \tag{12}$$

thus,

$$R = \frac{\sigma_B}{\sigma_e} = \frac{\sigma_e}{\sigma_w}. \tag{13}$$

For a given stress σ, we compute the limit void ratio $e_w(\sigma)$ from the w-line as:

$$e_w = e_N \exp\left[-\left(\frac{\sigma R}{h_s}\right)^n\right]. \tag{14}$$

Following Eq. (10) and (14), for a given void ratio e, the slope λ of all three lines (NCC, w-line and B-line) is identical.

Therefore, for $R = 1$, the w-line and the B-line coincide with the NCC.

In addition to e_w, the saturation driven strain rate further requires the limit void ratio e_s at the shrinkage limit w_s. For e_s we propose:

$$e_s = \begin{cases} (1+e_d)(\sigma_d/\sigma)^{\kappa_{\mathrm{ref}}} - 1 & \text{for } \sigma < \sigma_d, \\ e_d & \text{for } \sigma \geq \sigma_d. \end{cases} \tag{15}$$

2.7 Evolution equations for the state variables

In addition to the net stress, the proposed constitutive model introduces three variables (e, σ_d, e_d) to describe the current state. This section provides their corresponding evolution equations. Although the degree of saturation also determines the current state, the constitutive model handles it as a *given* variable because its evolution is governed by the mass balance at the finite element (and not at the material point) level.

The evolution of the void ratio is given by

$$\dot{e} = -(1+e)\dot{\epsilon}, \tag{16}$$

where changes of the void ratio are directly related to the *total* strain rate.

The preloading stress σ_d changes with the deformation and with the saturation. After long monotonic compression, σ_d increases and e_d decreases. They follow a path similar to first loading. On the other hand, experiments by Nitsch et al. [29] and Nowamooz and Masrouri [30] suggest that wetting processes reduce the preloading stress σ_d. In this case R reduces forcing both, the B-line and the w-line to move closer to the NCC. Therefore, we propose the following equation for the evolution of σ_d:

$$\dot{\sigma}_d = \dot{\sigma}_{d+} + \dot{\sigma}_{d-}, \tag{17}$$

where

$$\dot{\sigma}_{d+} = \frac{\sigma_d}{\lambda(e_d)}\left(\frac{\sigma_d}{\sigma}\right)^{-m}\dot{\epsilon}^h \tag{18}$$

is the buildup term due to loading beyond the preloading state and

$$\dot{\sigma}_{d-} = \frac{\sigma_e(e_d) - \sigma_d}{\lambda(e_d)}\left[-\dot{\epsilon}^w \cdot \frac{S^2}{c(e_w - e_s)} + S \cdot \dot{\epsilon}^h\right] \tag{19}$$

is the degradation term related to changes of the degree of saturation and loading under constant saturation. Notice the usage of the *total* degree of saturation S (instead of S^e) to capture the observation that even samples with very low degree of saturation $S^e \approx 0$ tend to approximate the NCC upon compression [30]. Only in the ideal case of a perfectly dry sample (with $S = 0$), the compression line will not approach the NCC. Finally, for the void ratio e_d corresponding to the preloading we propose:

$$\dot{e}_d = -(1+e)\left(\frac{\sigma_d}{\sigma}\right)^{-m}\dot{\epsilon}^h \tag{20}$$

In Eq. (20), e_d remains nearly constant upon unloading because $(\sigma_d/\sigma)^{-m}$ becomes negligible. For loading beyond

the preloading state, the factor $(\sigma_d/\sigma)^{-m}$ approaches 1 and e_d evolves in the same way as e. In this case Eq. (20) becomes nearly identical to Eq. (16), if the degree of saturation remains constant during that loading process.

2.8 Parameters of the model

The proposed constitutive model requires seven parameters, see Table 1, which can be determined from standard laboratory tests. Note that the exponent m for OCR is not considered as a model parameter, but is considered as a constant for all materials in the scope of this work. From the authors' experience, $m = 6$ produces an adequate transition from elastic to anelastic behavior.

The parameter calibration is explained in further detail in Sect. 4.

In addition to the material parameters, the initial state of the material described in Table 2 must be defined for every simulation.

3 Discussion of the model

In this section, the features of the proposed model are examined for different hydro-mechanical loading paths. All these loading paths are simulated with a single (arbitrary) set of material parameters. Most of the simulations include the preparation of the sample in the laboratory, which usually consists of two steps. First, the sample is statically loaded up to a certain stress σ_d at which the prescribed dry density, i.e. void ratio e_d, is reached. This state (σ_d, e_d) is denoted as the preloading of the sample (reference state at nearly dry $S = S^r$ conditions) and its evolution upon hydro-mechanical loading is tracked by the constitutive model. Before the actual test or simulation is run, the sample is unloaded to a stress $\sigma < \sigma_d$. Since the sample is *nearly* dry,

Table 1 Parameters for the constitutive model

Symbol	Description
Normal Compression Curve (NCC)	
e_N	Void ratio at $\sigma = 0$
h_s	Stress at inflection point of NCC
n	Exponent of Bauer equation
Elastic stiffness	
κ_{ref}	Unloading/Reloading slope for $S = S^r$
κ_w	Unloading/Reloading slope for $S = 1$
Watering	
b	Curvature for wetting and drying
Yielding	
c	Factor preloading degradation $\dot{\sigma}_{d-}$

Table 2 Initial conditions

Symbol	Description
$\sigma_{d,0}$	Initial preloading stress
$e_{d,0}$	Initial boid ratio corresponding to σ_d
σ_0	Initial net stress
e_0	Initial void ratio corresponding to σ_0
S_0	Initial degree of saturation

we assume that the void ratio after unloading corresponds to the void ratio at the shrinkage limit.

3.1 Oedometric compression under constant saturation

The response of the model (right) to loading and unloading paths at constant saturation for different initial degrees of saturation (left) are shown in Fig. 11. The path A-B-A* represents loading and unloading for the driest case possible ($S^e = 0$). The preloading state $(\sigma_{d,0}, e_{d,0})$, which lays on the B-line, marks the end of the elastic reloading. The slope of the subsequent loading line is affine to the slope $\lambda(e)$ of the NCC. With increasing degree of saturation, the NCC is reached sooner upon compression. This is achieved by the reduction of the preloading stress σ_d with the deformation (see Eq. (19)). For the simulation in the fully saturated state (I-J-I*), the compression path almost coincides with the NCC. Furthermore, the reduction of elastic stiffness according to Eq. (6) for both, reloading $\sigma \leq \sigma_d$ and unloading, can be clearly shown.

3.2 Saturation induced deformation

Figure 12 presents the response of the model to full saturation at constant-stress conditions. The compression curve and loading sequence for a test in the nearly dry state $S = S^r$ (A-B-A*) is shown as well to illustrate the loading history. Starting at $(\sigma_{d,0}, e_{d,0})$, the stress is reduced to points A, D, F and H. Then, the degree of saturation is increased while keeping the stress constant. The deformation reached in each simulation at the fully saturated state is determined by the position of the w-line. Hence, the points C, E, G and I coincide with the void ratio e_w according to Eq. (14). The saturation induced deformation decreases with the stress, which is achieved by the affinity of the w-line to the NCC.

3.3 Swelling pressure

Figure 13 presents response of the model to wetting at volume-constant conditions for different initial densities. After unloading from $(\sigma_{d,0}, e_{d,0})$ to A (nearly dry state
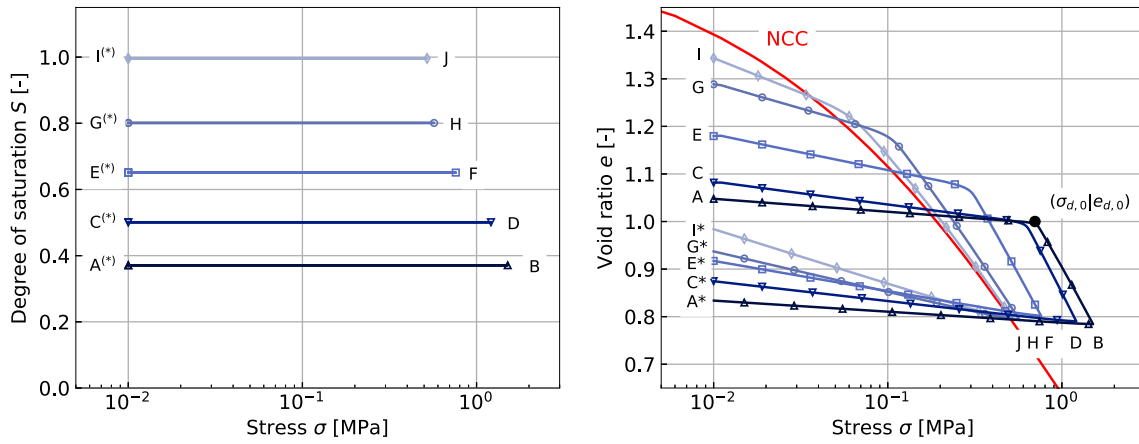
Fig. 11 Oedometric loading and unloading for different degrees of saturation
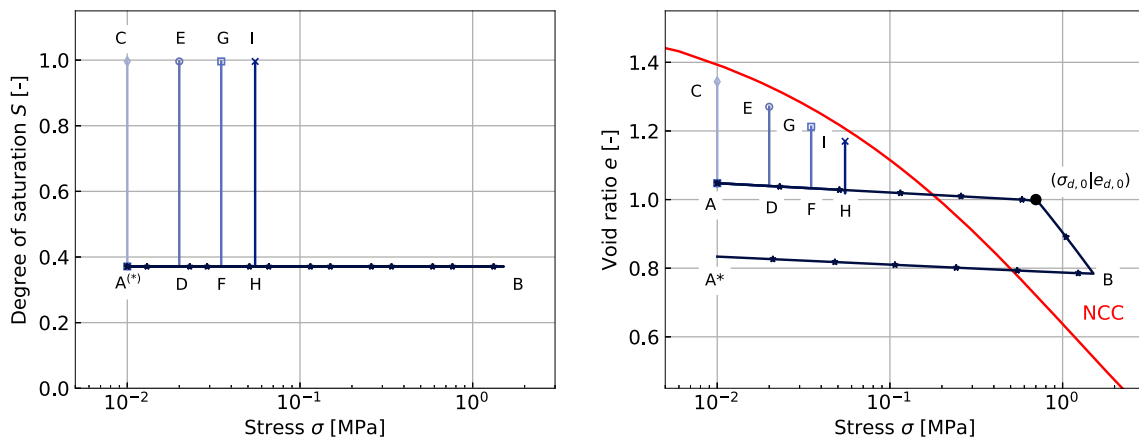

Fig. 12 Saturation induced deformation at different stresses: stress and wetting paths (left) and response of the model (right)
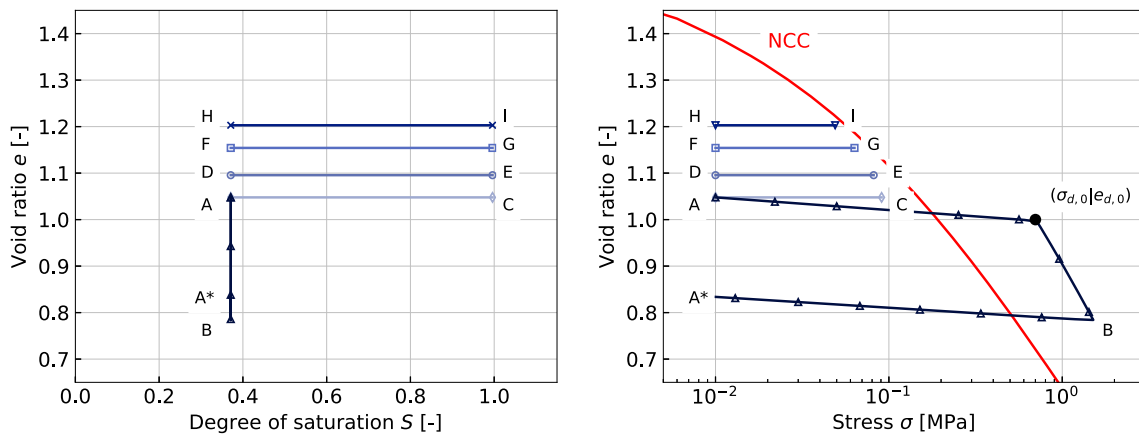

Fig. 13 Wetting induced swelling pressure (S=1) at different initial void ratios due to increments of degree of saturation: stress and wetting paths (left) and response of the model (right)

$S = S^r$), the degree of saturation was increased until $S = 1$. As reaction to the constant-volume constraint, the stress increases up to C. The states D, F, and H were reached by preparing the samples at lower preloading stresses (higher void ratios). The magnitude of the maximum swelling

pressure at points C, E, G and I in the fully saturated state is determined by the position of the w-line.

3.4 Collapse upon Wetting

Similar to the BBM [1], a transition point from swelling to collapse behavior exits in the proposed constitutive model. Collapse occurs when the stress at which wetting takes place is larger than the stress on the w-line for the current void ratio, i.e. $\sigma > \sigma_w(e)$. For this condition, the sign of the saturation driven strain rate in Eq. (8) becomes positive, because $e > e_w$. The response of the model for wetting induced collapse is shown in Fig. 14. The compression curve and loading sequence for a test in the nearly dry state $S = S^r$ (A-B-A*) is also shown. After a partial unloading from $(\sigma_{d,0}, e_{d,0})$, the degree of saturation was increased until $S = 1$ while the stress was kept constant. The deformation increases until the void ratio reaches its limit value $e = e_w$ (according to Eq. (14)) at point C on the w-line.

4 Determination of the material parameters and their significance

As described in Sect. 2.8, the proposed model requires seven parameters. The parameters of the model can be directly determined from the results of common laboratory tests apart from the watering parameter b and the yielding parameter c, whose significance will therefore be discussed in more detail. In the following, all laboratory tests refer to tests under oedometric conditions.

Note that together with the proposed constitutive model, the simulation of laboratory test require an additional hydraulic model which is not part of this work. Thus, the residual degree of saturation S^r and the van-Genuchten parameters α and n need to be specified as shown in the simulations of Sect. 5. A detailed method for the determination of the model parameters and the recommended laboratory tests are presented below.

The values of the parameters and typical ranges will be presented for three different materials in the following Sect. 5.

4.1 Parameters e_N, h_s, and n of the normal compression curve (NCC)

The NCC is the core of the model. Its three parameters can be best obtained simultaneously by fitting the Bauer equation (Eq. (3)) to the loading path of an oedometer test preceded by unconfined swelling up to full saturation or two the respective parts of the loading paths of two separate tests. However, the parameters can be individually adjusted to match specific laboratory tests. For example, the void ratio e_N at zero net stress can be estimated from an unconfined axial swelling strain test conducted at a very low stress level. Compression tests up to very large stresses can be used to estimate the stress at the inflection point h_s of the NCC. Also the exponent n can be adjusted from such tests. Since for a given void ratio e the maximum swelling pressure $\sigma_{\max}$ should always be smaller than the equivalent stress $\sigma_e(e)$, the plausibility of the position of the NCC can be validated by swelling pressure tests.

4.2 Swelling indexes κ_{ref} and κ_w

To compute the elastic stiffness σ/κ of the model (see Eq. (7)), the saturation dependent swelling index $\kappa = \kappa(S)$ is interpolated from the constants κ_{ref} and κ_w, see Eq. (6). The swelling index κ_{ref} can be directly obtained from unloading paths of an oedometer test at the driest possible state. The swelling index κ_w can be calibrated by means of an oedometer test on a full saturated sample or from the
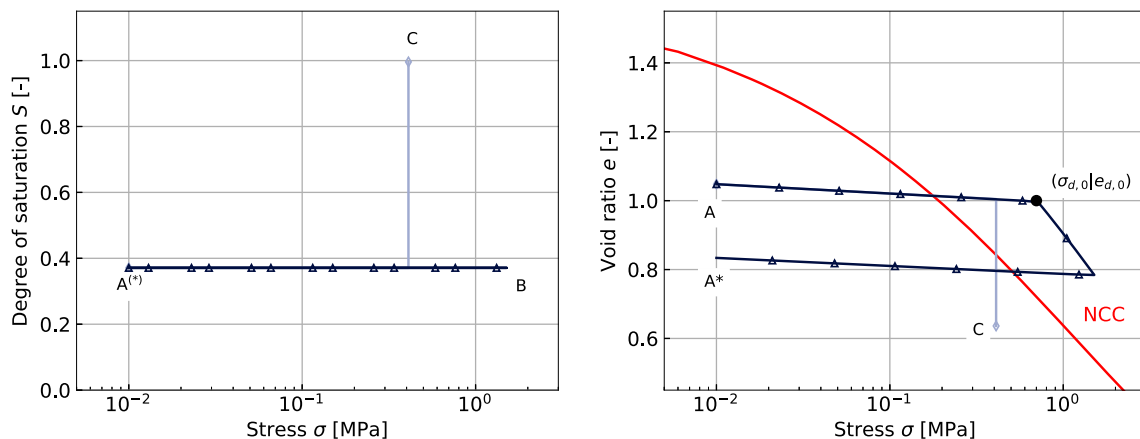

Fig. 14 Wetting induced collapse (S=1) due to increments of degree of saturation: stress and wetting paths (left) and response of the model (right)

unloading path of a multi-step swelling test under oedometric conditions, e.g. following the Huder-Amberg-method [16].

4.3 Parameter b for the Evolution of the Saturation Driven Strain

The parameter b controls the evolution of the strain upon changes in the degree of saturation, see Eq. (8). The parameter b can be found from a back-calculation of an unconfined axial swelling strain test. In the $\epsilon - S-$space, unconfined swelling results in an around its inflection point point-symmetrical sigmoid-shaped path (similar to Fig. 5). For small values of b, the inflection point of this path occurs at high degrees of saturation. If b is too small, the limit void ratio e_w may not be reached at full saturation and the saturation driven strain may be underestimated. For large values of b the evolution of the saturation strain flattens out prematurely and may also be underestimated. Since the limit void ratio e_w in Eq. (8) depends on the preloading–and therefore on the parameter c–, both b and c should be simultaneously optimised. For a first estimation of b, a value of $c = 1.0$ can be chosen.

4.3.1 Significance of b

The influence of different values for b on the evolution of the horizontal distance $R = \sigma_B/\sigma_e$ between B-line/w-line and NCC, hence the evolution of the bounding stress σ_B, and on the deformation upon wetting during an unconfined axial swelling strain test ($S = 1$) are shown in Fig. 15. Note that the parameter for yielding is chosen arbitrarily as $c = 2.6$ in all three calculations. No unique trend can be observed with a variation of b, since not only the curvature of the sigmoid-function, but also the final value is influenced by the parameter b. With increasing b the inflection point of the $e - w$-curve is shifted to a lower water content,

therefore an pronounced plateau can be observed, and the deformation does not reach its final value ($b = 50$, lightest curve in Fig. 15, right). In contrast, with a small value for b the inflection point may not yet be reached and the $e - w$-curve does not flatten ($b = 5$, darkest curve in Fig. 15, right). Both extreme values are not able to reproduce the deformation upon wetting correctly and underestimate the deformation due to wetting, see Fig. 15, left and right. The same observation can be made for the reduction of bounding stress upon wetting, see Fig. 15, center. For the studied material, the medium value $b = 17$ produces a well shaped sigmoid-function for the evolution of deformation with watering and thus for the evolution of $R = \sigma_B/\sigma_e$ as well.

4.4 Parameter c associated with yielding

The constant c, which controls the evolution of the preloading pressure σ_d with the saturation and the deformation (see Eq. (19)), should be determined as the last parameter, but optimised together with b. The parameter c strongly impacts the prediction of stress/strain at fully and partially saturated conditions. For a preliminary determination, at least one confined and one unconfined swelling test (ideally followed by oedometric loading) are required. Having a first estimation of b, the parameter c must then be chosen in such a way, that the magnitude of the deformation upon wetting in the partially saturated state as well as the slope of the subsequent oedometric compression path (see Fig. 2) are simulated correctly. Further improvements require a gradual and simultaneous adjustment of b and c.

4.4.1 Significance of c

A clear influence of the parameter c for yielding on the evolution of $R = \sigma_B/\sigma_e$ and on the deformation upon
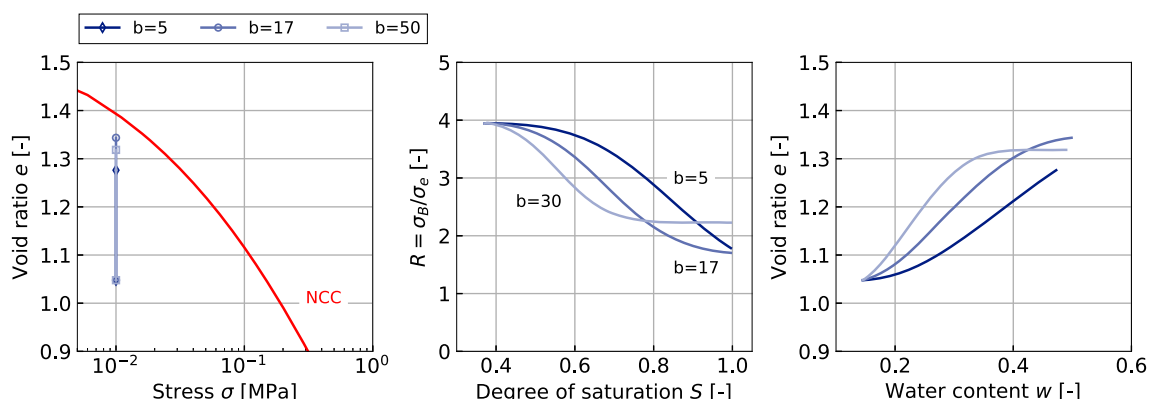
Fig. 15 Influence of wetting parameter b during volumetric deformation (S=1): deformation (left), horizontal distance $R = \sigma_B/\sigma_e$ between B-line/w-line and NCC (center) and void ratio vs. water content (right)
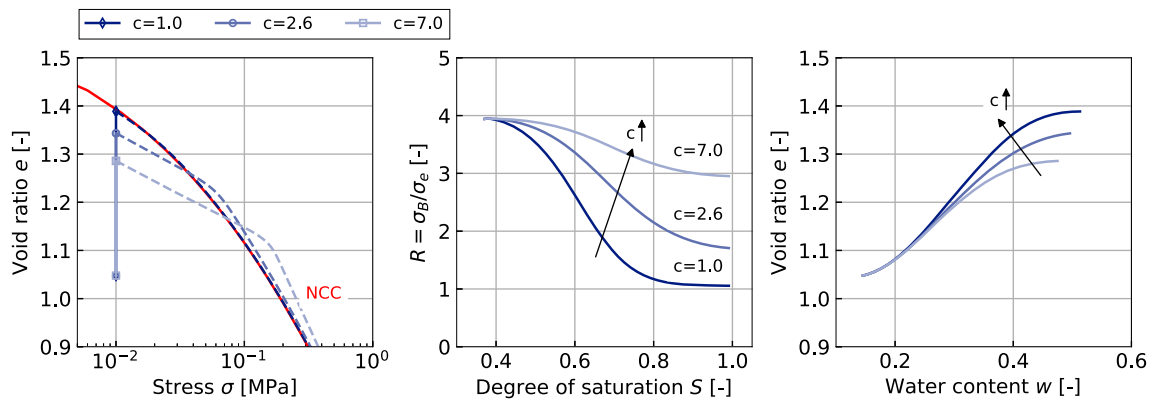
Fig. 16 Influence of yielding parameter c during volumetric deformation (S=1): deformation (left), horizontal distance $R = \sigma_B/\sigma_e$ between B-line/w-line and NCC (center) and void ratio vs. water content (right)

wetting can be seen in Fig. 16 during an unconfined axial swelling strain test. Note that the value of $b = 17$ was chosen in all three calculations, i.e. the medium dark curves correspond to each other in Fig. 15 and 16. An additional oedometric compression is added to the calculations to clearly evaluate the influence on the preloading pressure, hence the transition from elastic to unelastic material behavior. For the sake of clarity, the compression paths are only shown in Fig. 16, left (dashed lines). With an reduction of R, the B-line is shifted closer to the NCC and thus also the w-line at the same time.

For $c = 1.0$ the evolution of the bounding stress σ_B and preloading stress σ_d are most pronounced and their reduction takes place very fast. With increasing c the reduction of R is slowed down (Fig. 16, center) and a smaller deformation takes place.

The influence of c becomes clear during the whole wetting process. As a consequence not only the fully saturated material behavior is strongly dependent on the magnitude of c, but also the partially saturated behavior. Without slowing the reduction of R down, hence $c = 1.0$ the evolution of R is already complete for partially saturated conditions ($c = 1.0$, darkest curve in Fig. 16). As a consequence, a fully and partially saturated test do not distinguish in the transition point from elastic to anelastic behavior, nor in the magnitude of the deformation. With an increase of c the reduction of R becomes so slow, that the differences for partial saturation are not significant enough and both, the transition point from elastic to anelastic behavior, and the magnitude of deformation upon wetting, do not differ enough overall ($c = 7.0$, lightest curve in Fig. 16). In both cases, the material behavior which is commonly observed during unconfined swelling and oedometric loading of partially saturated samples cannot be reproduced. For the studied material, the medium value $c = 2.6$ produces a well shaped $R - S$-curve (see Fig. 16),

center and is also suited to predict partially saturated behavior.

5 Simulation of laboratory tests

To evaluate its performance, a set of laboratory tests on three different expansive materials is simulated using the proposed model. The experiments include the most representative hydro-mechanical loading paths. Hence, the simulations focus, among others, on the prediction of the maximum swelling strain and stress upon full saturation, the reduction of stiffness with increasing degree of saturation, and the overall mechanical material response to subsequent oedometric loading/unloading paths.

For each material, a single set of material parameters was used to simulate all the experiments. Since the suction was controlled in some of the experiments, a simple soil water retention curve SWRC after Van Genuchten [41] was used to relate the suction with the degree of saturation (which was required by the constitutive model).

5.1 Tests on reconstituted opalinus clay shale

The experimental campaign by Nitsch et al. [29] focussed mainly on the swelling behavior of reconstituted Opalinus clay shale (with 5% smectite and 32% illite content) and its influence on the mechanical behaviour during monotonic loading and unloading. Starting from nearly dry states, samples with similar void ratios were fully saturated and then subjected to oedometric loading and unloading paths. The saturation occurred under different conditions: (a) constant-volume (swelling pressure test, OPA-0-34); (b) constant-volume (swelling pressure test, OPA-0-07) followed by unloading; and (c) constant-stress (unconfined axial swelling strain test, OPA-0-24). For comparison,
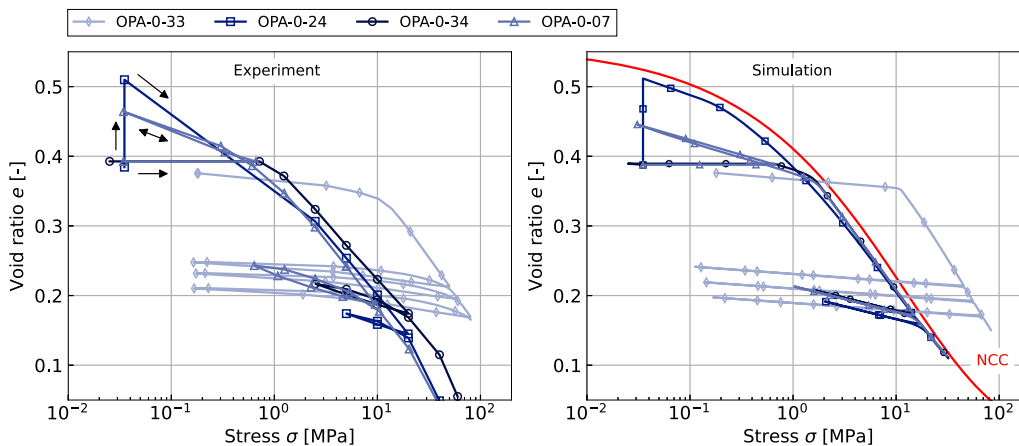
Fig. 17 Simulation of oedometric compression tests preceded by different swelling phases after [29]

another sample was loaded at dry conditions (without the saturation stage, OPA-0-33).

Figure 17 shows the simulations (right) of the experiments (left) on reconstituted Opalinus clay shale. The material constants and the initial conditions used in the simulations are listed in Tables 3 and 6, respectively. The model is able to predict the mechanical response in the dry state and after different wetting paths with subsequent oedometric loading and unloading. The experiments support the hypothesis of a unique NCC after long monotonic compression, see Sect. 2.2. The similar slope $\lambda(e)$ of the NCC and the loading branch of the test on nearly dry material (OPA-0-33), which corresponds to the B-line, can be clearly identified. The pronounced increase of the unloading/reloading slope from the reference κ_{ref} state to the saturated κ_w conditions can be clearly observed in the experiments, see Sect. 2.3. The results show that the model is able to reproduce both the maximum swelling pressure and the maximum swelling strain with a single set of material parameters.

5.2 Tests on partially saturated bentonite-silt mixtures

In an extensive experimental campaign, Nowamooz and Masrouri [30, 31] reported suction-controlled wetting tests followed by oedometric compression on a Silt-Bentonite-

Table 3 Initial conditions for the simulations on Opalinus clay shale from Nitsch et al. [29]

	$\sigma_d, 0$ (MPa)	$e_{d,0}$	σ_0 (MPa)	e_0	$S_0 = S^r$
OPA-0-33	10.535	0.359	0.18	0.376	0.13
OPA-0-24/07	10.535	0.359	0.035	0.388	0.13
OPA-0-34	10.535	0.359	0.025	0.387	0.13

**Table 4** Initial conditions for tests on a Bentonite-Silt-Mixture from Nowamooz and Masrouri [30]

	$\sigma_{d,0}$ [MPa]	$e_{d,0}$ [-]	σ_0 [MPa]	e_0 [-]	S_0 [-]
M1	0.700	1.001	0.010	1.047	0.371
M4	0.540	1.051	0.010	1.095	0.371
M5	0.488	1.071	0.010	1.102	0.371

Mixture with 62 % montmorillonite. Figure 19 compares the experiments (left) of with the simulations (right) performed with the proposed model. The material constants and the initial conditions for the simulations are listed in Tables 4 and 6, respectively. Starting from a similar initial stress and void ratio, the samples were subjected to different increments of saturation while keeping the net stress constant. The sample M1 reached full saturation while samples M4 and M5 reached lower degrees of saturation: $S = 0.79$ and $S = 0.54$, respectively. The swelling stage was followed by oedometric compression up to 1 MPa and finally by oedometric unloading.

Since the degree of saturation is a driving variable for the simulations, the suction-controlled conditions of the experiments had to be transformed into saturation-controlled ones. This was achieved by using a simple soil water retention curve SWRC as a *one-to-one* suction-saturation relationship. The SWRC resulted by fitting the experimental data, i.e. suction measurements for six different water contents, to the van Genuchten Eq. (21) with constants $\alpha = 0.361, n = 2.026, S^r = 0.261$:

$$S = S^r + (1 - S^r) \left(\frac{1}{1 + (\alpha \cdot s)^n} \right)^{1 - \frac{1}{n}}. \tag{21}$$
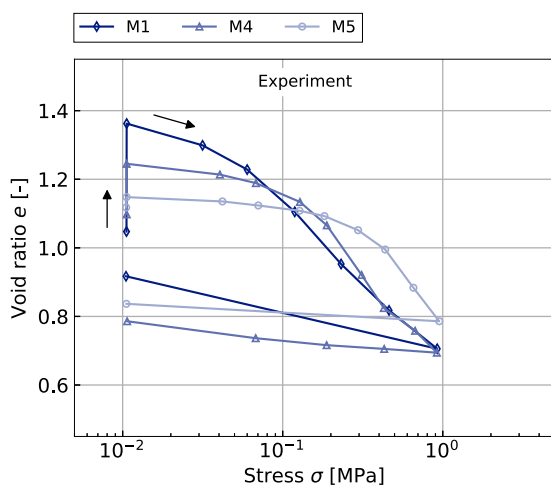
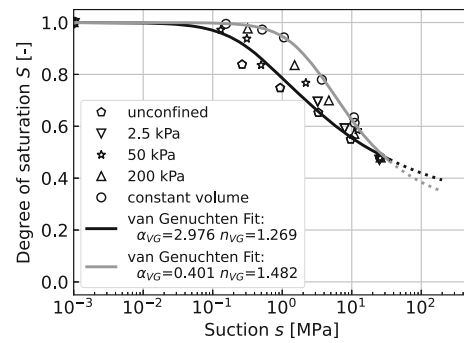The experimental data and van Genuchten fit is shown in Fig. 18.
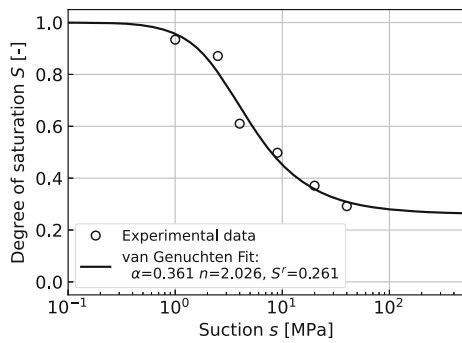
Fig. 18 Soil water retention curve (SWRC): experimental data from Nowamooz and Masrouri [30] and van Genuchten fit

Fig. 20 Soil water retention curve: experimental data from [20] and van Genuchten Fit for unconfined (black) and confined (grey) conditions

The simulations show that the NCC was reached after a long monotonic loading path for all tests. Both the stiffness of the loading paths and preconsolidation stress are well reproduced by the model. The simulations further show the reduction of elastic stiffness with an increasing degree of saturation.

The magnitude of the strain during wetting is not optimally reproduced by the model for all tests. This can be attributed to uncertainties in the data supporting the SWRC and to the assumption of a simple hydraulic model. However, the model is able to qualitatively reproduce the increasing deformation with increasing degree of saturation. In summary, the model can satisfactorily simulate the main features of partially saturated unconfined swelling and the subsequent oedometric compression with a single set of material parameters.

Table 5 Initial conditions for tests on a Bentonite-Sand-Mixture from Lang [20]

	$\sigma_{d,0}$ [MPa]	$e_{d,0}$ [-]	σ_0 [MPa]	e_0 [-]	S_0 [-]
BS-SCR-1-4, BS-WCV-1/5/7	10.2	0.498	0.025	0.530	0.468

5.3 Tests on partially saturated Sand-Bentonite mixtures

Lang [20] conducted a large number of experiments on Sand-Bentonite-mixtures with $30 - 35\%$ montmorillonite content using different stress and saturation paths.

To evaluate the performance of the proposed model, swelling strain and swelling pressure tests with subsequent oedometric loading have been simulated.

Fig. 19 Simulation of swelling strain and oedometric compression test on partially and fully saturated samples after Nowamooz and Masrouri [30]

Table 6 Model parameters for three experimental campaigns and typical range. The respective content of high-swellable clay minerals is given in brackets

Parameter	Typical range	Opalinus Clay [29] (5%)	Bentonite-Sand-Mix[20] (30 − 35%)	Bentonite-Silt-Mix [30] (62 %)
e_N	$0.5 - 1.8$	0.58	0.895	1.615
h_s [MPa]	$1 - 25$	9.0	18.0	1.2
n	$0.30 - 0.45$	0.40	0.31	0.40
κ_{ref} [10^{-3}]	$0.5 - 5$	3.792	1.103	2.017
κ_w [10^{-3}]	$2 - 20$	13.59	7.044	26.47
c	$2 - 10$	4.5	5.0	2.6
b	$15 - 60$	55	15	17

Lang also investigated the dependency of the soil water retention curves on the net stress. Among all the SWRCs, two extreme cases were fitted to the van Genuchten Eq. (21): one for unconfined (zero stress) (black, $\alpha = 2.976, n = 1.269$) and other for confined (increasing stress) (grey, $\alpha = 0.401, n = 1.482$) conditions, as shown in Fig. 20. The residual degree of saturation was $S^r = 0.26$. The material constants and the initial conditions for the simulations are listed in Tables 5 and 6, respectively.

Figure 21 compares the experiments (left) with the simulations (right) performed with the proposed model for unconfined swelling with subsequent oedometric loading and unloading. The van Genuchten fit for unconfined conditions was used for these calculations. Prior to the oedometric loading, the samples reached different degrees of saturation upon constant stress conditions: BS-SCR-1

($S = 1.0$), BS-SCR-2 ($S = 0.64$), BS-SCR-3 ($S = 0.55$), and BS-SCR-4 ($S = S^r = 0.26$).

Similar to the previous Sections 5.1 and 5.2, the magnitude of deformation, the stiffness of the loading and unloading/reloading paths, and the magnitude of the pre-consolidation stress are well reproduced by the model. With increasing degree of saturation, the NCC is approached more rapidly and the reduction of the unloading stiffness is more pronounced.

Figure 22 compares the results of swelling pressure tests for different saturation degrees (left) with their simulations using the SWRC for confined conditions (right). In the experiments (left), each of the reached swelling pressures corresponds to a final value of suction. For the simulation however, suction was transformed to saturation through the SWRC for confined conditions (right). To illustrate the influence of the chosen SWRC on the model's performance, Fig. 22 (center) presents the simulation results using the SWRC for unconfined conditions.

As it can be observed, the swelling pressure in the fully saturated state is well predicted, but both simulations show significant deficits for the prediction of swelling pressure in the partially saturated states. With the unconfined SWRC (Fig. 22, center) the swelling pressure for small degrees of saturation is underestimated (BS-WCV-7), but well predicted for higher degrees of saturation (BS-WCV-5) and full saturation (BS-WCV-1). In contrast, with the confined SWRC (Fig. 22, right), the prediction is better for lower degrees for saturation. This shows that the quality of the hydraulic model needs to be as good as the quality of the constitutive model in order to achieve good predictions of swelling pressure tests under partially saturated conditions.
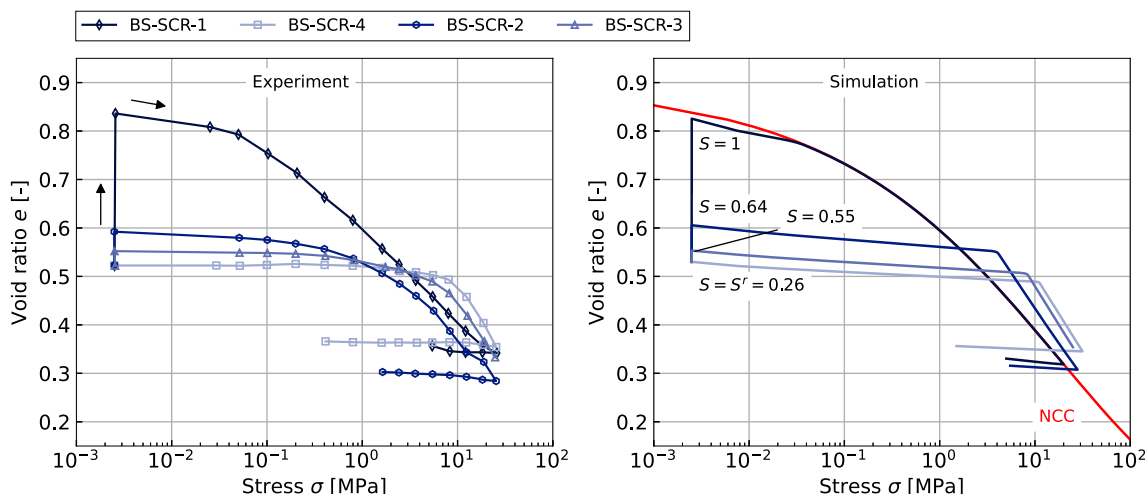
Fig. 21 Simulation of swelling strain and oedometric compression test on partially and fully saturated samples after Lang [20]: (**a**) Experiments and (**b**) NCC and Simulation
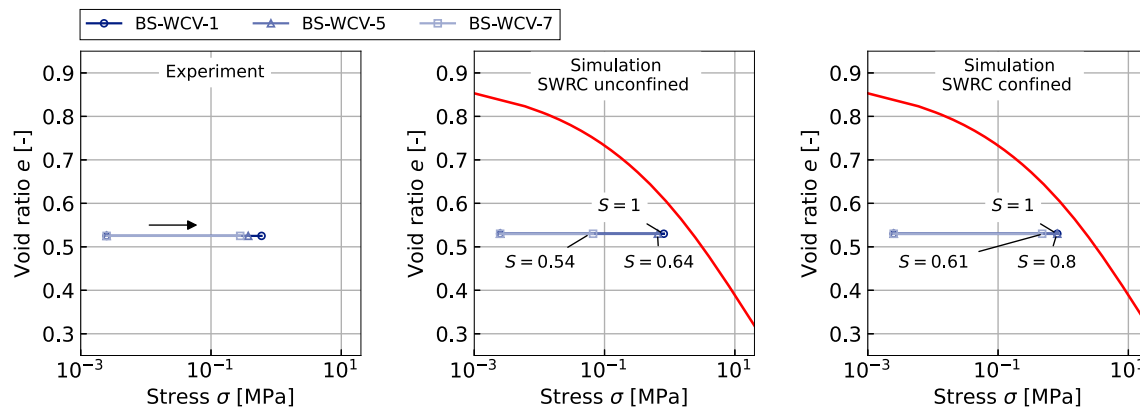
Fig. 22 Simulation of swelling pressure on partially and fully saturated samples after Lang [20]: Experiments (left) and simulations using unconfined SWRC (center) and confined SWRC (right)

5.4 Remarks on model parameters

As Table 6 shows, a typical range can be given for the parameters based on the validation of the constitutive model on three materials. The exponent for OCR was chosen as $m = 6$ for all tests.

The typical range of some of the model parameters, e.g. the void ratio e_N at zero stress of the Bauer Eq. (3), can be associated with the range of content of high-swellable clay minerals from the presented materials. Other model parameters seem to be almost independent of the type of expansive material, e.g. the curvature parameter n of the Bauer-Eq. (3).

In the past efforts have been made by e.g. [19, 35, 44] amongst others to compute the swelling pressure depending on the montmorillonite or bentonite content of a material. Various approaches have proven to be suitable. Since the swelling pressure development is only one of the responses to the swelling mechanism in the proposed model, that is for confined boundary conditions, it is assumed that the entire response of a material subjected to hydro-mechanical loading can be related to the amount of expansive clay minerals in the material. Further investigations are required to support this thesis.

6 Conclusions

- The proposed model is able to reproduce essential features of the behaviour of partially saturated expansive soils under oedometric conditions. Among others, processes like swelling, wetting/drying at constant volume, monotonic loading, and reversible unloading/reloading for samples at different degrees of saturation can be simulated with a single set of material constants.

Also the volumetric collapse, i.e. the reduction of the void ratio upon wetting, can be captured by the model.
- Oedometric tests with varied hydro-mechanical loading paths on three different expansive materials could be satisfactorily simulated by the model.
- Whereas the maximum swelling strain and the maximum swelling pressure can be predicted with a simple soil water retention curve, a more sophisticated approach to the hydraulic model is required to simulate the swelling pressure at partially saturated conditions due to the dependency of the SWRC on the stress and void ratio.
- The basic ideas of the model – that is, a saturation driven strain rate, the dependence of stiffness on the degree of saturation, and state variables tracking the loading history – can be extended to formulate three dimensional constitutive models. The promising results of the 1D version of the model motivate the extension to a 3D formulation, which is in the scope of future work.

Declarations

References

1. Alonso EE, Josa AG (1990) A constitutive model for partially saturated soils. Géotechnique 40(3):405–430

2. Alonso EE, Vaunat J, Gens A (1999) Modelling the mechanical behaviour of expansive clays. Eng Geol 54(1):173–183. https://doi.org/10.1016/S0013-7952(99)00079-4

3. Anagnostou G (1993) A model for swelling rock in tunnelling. Rock Mech Rock Eng 26(4):307–331

4. Baille W, Tripathy S, Schanz T (2010) Swelling pressures and one-dimensional compressibility behaviour of bentonite at large pressures. Appl Clay Sci 48(3):324–333. https://doi.org/10.1016/j.clay.2010.01.002

5. Bauer E (1996) Calibration of a comprehensive hypoplastic model for granular materials. Soils Foundations 36:13–26. https://doi.org/10.3208/sandf.36.13

6. Bosch J, Ferrari A, Laloui L (2020) A coupled hydro - mechanical approach for modelling the volume change behaviour of compacted bentonite. E3S Web of Conferences 195:04006. https://doi.org/10.1051/e3sconf/202019504006

7. Butterfield R (1979) Natural compression law for soils (an advance on e-log p)'. Geotechnique 29:469–480. https://doi.org/10.1680/geot.1979.29.4.469

8. Delahaye CH, Alonso EE (2002) Soil heterogeneity and preferential paths for gas migration. Eng Geol 64(2):251–271. https://doi.org/10.1016/S0013-7952(01)00104-1

9. Della Vecchia G, Dieudonné A-C, Jommi C, Charlier R (2015) Accounting for evolving pore size distribution in water retention models for compacted clays. Int J Numer Anal Meth Geomech 39(7):702–723. https://doi.org/10.1002/nag.2326

10. Dieudonne A-C, Della Vecchia G, Charlier R (2017) Water retention model for compacted bentonites. Can Geotech J 54(7):915–925. https://doi.org/10.1139/cgj-2016-0297

11. Estabragh AR, Parsaei B, Javadi AA (2015) Laboratory investigation of the effect of cyclic wetting and drying on the behaviour of an expansive soil. Soils Found 55(2):304–314. https://doi.org/10.1016/j.sandf.2015.02.007

12. Gens A, Alonso EE (1992) A framework for the behaviour of unsaturated expansive clays. Can Geotech J 29(6):1013–1032. https://doi.org/10.1139/t92-120

13. Grob H (1972) Schwelldruck im Belchentunnel. In: Proceedings international symposium Für Untertagebau, Luzern, pp 99–119

14. Hanafy EADE (1991) Swelling/shrinkage characteristic curve of desiccated expansive clays. Geotech Test J 14(2):206–211. https://doi.org/10.1520/GTJ10562J

15. Heidkamp H, C K (2004) The swelling phenomenon of soils - Proposal of an efficient continuum modelling approach. EUROROCK 2004 and 53rd Geomechanics Colloquium

16. Huder J, Amberg G (1970) Quellung in mergel, opalinuston und anhydrit. Schweizerische Bauzeitung 88(43):975. https://doi.org/10.5169/seals-84648

17. Jadda K, Bag R (2020) Effect of initial compaction pressure and elevated temperature on swelling pressure of two indian bentonites. Environm Earth Sci, 79(197) https://doi.org/10.1007/s12665-020-08937-0

18. Klobe B (1992) Eindimensionale Kompression und Konsolidation und darauf basierende Verfahren zur Setzungsprognose. PhD

19. thesis, Institut für Boden und Felsmechanik der Universität Karlsruhe, Heft 128

19. Komine H, Ogata N (2003) New equations for swelling characteristics of bentonite-based buffer materials. Can Geotech J 40(2):460–475. https://doi.org/10.1139/t02-115

20. Lang L (2019) Hydro-mechanical behaviour of bentonite-based materials used for disposal of radioactive wastes. PhD thesis, Ruhr-Universität Bochum

21. Liu Martin D, Suched L, Suksun H, Huy ND (2021) 1d constitutive model for expansive soils. Int J Geomech 21(3):04020260. https://doi.org/10.1061/(ASCE)GM.1943-5622.0001921

22. Lloret A, Villar M, Sánchez M, Gens A, Pintado X, Alonso E (2003) Mechanical behaviour of heavily compacted bentonite under high suction changes. Géotechnique. https://doi.org/10.1680/geot.53.1.27.37258

23. Mašín D, Khalili N (2008) A hypoplastic model for mechanical response of unsaturated soils. Int J Numer Anal Meth Geomech 32(15):1903–1926. https://doi.org/10.1002/nag.714

24. Middelhoff M, Cuisinier O, Masrouri F, Talandier J, Conil N (2019) Combined impact of selected material properties and environmental condi- 1 tions on the swelling pressure of compacted claystone/ bentonite mixtures. Appl Clay Sci https://doi.org/10.1016/j.clay.2019.105389

25. Mohajerani M, Delage P, Monfared M, Tang A-M, Sulem J, Gatmiri B (2011) Oedometric compression and swelling behaviour of the callovo-oxfordia, argillite. Int J Rock Mech Min Sci 48:606–615. https://doi.org/10.1016/j.ijrmms.2011.02.016

26. Monroy R, Zdravkovic L, Ridley A (2010) Evolution of microstructure in compacted london clay during wetting and loading. Géotechnique 60(2):105–119. https://doi.org/10.1680/geot.8.P.125

27. Niemunis A (2003) Extended hypoplastic models for soils. PhD thesis, Ruhr-Universität Bochum, Heft 34

28. Niemunis A, Grandas-Tavera CE, Prada-Sarmiento LF (2009) Anisotropic visco-hypoplasticity. Acta Geotech 4:293–314. https://doi.org/10.1007/s11440-009-0106-3

29. Nitsch A, Leuthold J, Machacek J, Wichtmann T, Grandas C (2021) Experimental investigations of the stress-dependent swelling behavior of reconstituted claystone. In: Fachsektionstage Geotechnik 2021: 24. Symposium Felsmechanik und Tunnelbau

30. Nowamooz H, Masrouri F (2008) Hydromechanical behaviour of an expansive bentonite/silt mixture in cyclic suction-controlled drying and wetting tests. Eng Geol 101:154–164. https://doi.org/10.1016/j.enggeo.2008.04.011

31. Nowamooz H, Masrouri F (2009) Density-dependent hydromechanical behaviour of a compacted expansive soil. Eng Geol 106:105–115. https://doi.org/10.1016/j.enggeo.2009.03.010

32. Olszak W, PP (1966) The constitutive equations of the flow theory for a nonstationary yield condition. In: Applied Mechanics, Proceedings of the 11th international congress, pp 545–553

33. Romero E, Della Vecchia G, Jommi C (2011) An insight into the water retention properties of compacted clayey soils. Géotechnique 61(4):313–328. https://doi.org/10.1680/geot.2011.61.4.313

34. Roscoe K, BJ (1968) On the generalized stress-strain behaviour of wet clays. Engineering Plasticity, 535–609

35. Samingan A, Schanz T (2008) A method for predicting swelling pressure of compacted bentonites. Acta Geotech 3:125–137. https://doi.org/10.1007/s11440-008-0057-0

36. Sánchez M, Gens A, Olivella S (2012) Thm analysis of a large-scale heating test incorporating material fabric changes. Int J Numer Anal Meth Geomech 36(4):391–421. https://doi.org/10.1002/nag.1011

37. Schanz T, Tripathy S (2009) Swelling pressure of a divalent-rich bentonite: Diffuse double-layer theory revisited. Water Resour. Res. 45(5). https://doi.org/10.1029/2007WR006495

38. Seiphoori A, Moradian Z, Einstein HH, Whittle AJ (2016) Microstructural characterization of opalinus shale, 4:2742–2750. https://www.scopus.com/inward/record.uri?eid=2-s2.0-85010301140&partnerID=40&md5=ed9dbc6bd06db03d70c8ef6618fa7aeb

39. Toprak E, Olivella S, Pintado X (2018) Modelling engineered barriers for spent nuclear fuel repository using a double-structure model for pellets. Environm Geotech 7(1):72–94. https://doi.org/10.1680/jenge.17.00086

40. Tripathy S, Rao KSS, Fredlund DG (2002) Water content - void ratio swell-shrink paths of compacted expansive soils. Can Geotech J 39(4):938–959. https://doi.org/10.1139/t02-022

41. van Genuchten MT (1980) A closed-form equation for predicting the hydraulic conductivity of unsaturated soils. Soil Sci Soc Am J 44(5):892–898. https://acsess.onlinelibrary.wiley.com/doi/pdf/10.2136/sssaj1980.03615995004400050002x

42. Vaunat J, Gens A (2005) Analysis of the hydration of a bentonite seal in a deep radioactive waste repository. Eng Geol 81(3):317–328. https://doi.org/10.1016/j.enggeo.2005.06.014

43. Villar MV, Lloret A (2008) Influence of dry density and water content on the swelling of a compacted bentonite. Appl Clay Sci 39(1):38–49. https://doi.org/10.1016/j.clay.2007.04.007

44. Zeng Z, Cui Y-J, Talandier J (2021) Investigating the swelling pressure of highly compacted bentonite/sand mixtures under constant-volume conditions. Acta Geotechnica. https://doi.org/10.1007/s11440-021-01352-0

45. Zou W.-l, Han Z, Ye J.-b (2020) Influence of external stress and initial density on the volumetric behavior of an expansive clay during wetting. Environm Earth Sci 79(10):211. https://doi.org/10.1007/s12665-020-08960-1